



1 **Postmidnight equatorial plasma irregularities on June solstice during low solar activity**

2 **– a case study**

3

4 Claudia M. N. Candido^{1,2}, Jiankui Shi¹, Inez S. Batista², Fabio Becker-Guedes², Emília
5 Correia^{2,6}, Mangalathayil A. Abdu^{2,4}, Jonathan Makela³, Nanan Balan⁷, Narayan
6 Chapagain⁵, Chi Wang¹, Zhengkuan Liu¹

7

8 ¹National Space Science Center, NSSC, Chinese Academy of Sciences, State Key
9 Laboratory, China-Brazil Joint Laboratory for Space Weather, China

10 ²National Institute for Space Research – INPE, - São José dos Campos, SP, Brazil

11 ³Department of Electrical and Computer Engineering, University of Illinois at Urbana-
12 Champaign, Urbana, Illinois 61801, U.S.A

13 ⁴Instituto Tecnológico de Aeronáutica – ITA – São Jose dos Campos, Brazil

14
15 ⁵Department of Physics, Patan Multiple Campus, Tribhuvan University, Latitpur, Nepal.

16
17 ⁶Centro de Radio Astronomia e Astrofísica Mackenzie, CRAAM, University Presbiteriana
18 Mackenzie – São Paulo – Brazil

19

20 ⁷Institute of Geology and Geophysics, Chinese Academy of Sciences, Beijing 100029,
21 China

22

23

24 Corresponding author: claudia.candido@inpe.br

25

26 *Keywords:* Solar minimum, Spread-F, Postmidnight plasma irregularities, equatorial
27 ionosphere, ionosonde

28

29

30

31



32 **Abstract**

33

34 We present a case study of unusual spread-F structures observed by ionosondes at two
35 equatorial and low latitude Brazilian stations - Sao Luis (SL: 44.2° W, 2.33° S, dip angle:
36 -6.9°) and Fortaleza (FZ: 38.45°W, 3.9° S, dip angle: -16°). The irregularity structures
37 observed from midnight to post-midnight hours of moderate solar activity ($F_{10.7} < 97$) have
38 characteristics different from typical post-sunset equatorial spread-F. The spread-F traces
39 first appeared at or above the F-layer peak and gradually became well-formed mixed spread-
40 F. They also appeared as plasma depletions in the 630.0 nm airglow emissions made by a
41 wide-angle imager located at nearby low latitude station Cajazeiras (CZ: 38.56° W, 6.87° S,
42 dip angle: -21.4°). The irregularities appeared first over FZ and later over SL, giving
43 evidence of an unusual westward propagation or a horizontal plasma advection. The drift
44 mode operation available in one of the ionosondes (a Digital Portable Sounder, DPS-4) has
45 enabled us to analyze the horizontal drift velocities and directions of the irregularity
46 movement. We also analyzed the neutral wind velocity measured by a Fabry-Perot
47 interferometer (FPI) installed at CZ and discussed its possible role on the development of
48 the irregularities.

49

50 **1 Introduction**

51

52 Equatorial spread-F representing small scale to large scale plasma irregularities has been
53 extensively studied for several decades. The large-scale plasma irregularities specifically
54 known as equatorial plasma bubbles (EPBs) are known to be associated with equatorial
55 spread-F. In the Brazilian equatorial sector, characterized by large negative magnetic
56 declination, spread-F and EPBs have high occurrence rates during local summer and
57 equinoctial months (Abdu et al., 1981; Sahai et al., 2000; Sobral et al., 2002). However,



58 during low solar activity conditions, there is a class of spread-F/plasma irregularities
59 regularly observed in distinct longitudinal sectors. They are known as post-midnight plasma
60 irregularities (PMIs), which occur mostly in June solstice. A recent review of plasma
61 irregularities is provided by Balan et al. (2018).

62 PMIs occur under conditions considered not favorable for the development of the Rayleigh-
63 Taylor (RT) instability, since that at night the vertical plasma drifts are downward, owing to
64 the westward electric fields. In recent years, a variety of works have reported their
65 occurrence both at low latitudes and equatorial region. Otsuka et al. (2009) and Nishioka et
66 al. (2012) investigated PMIs over Indonesia and discussed their possible sources. Li et al.
67 (2011) reported these irregularities observed over Hainan, China during low solar activity.
68 Candido et al. (2011) presented a study of PMIs observed over the south crest of the
69 equatorial ionization anomaly (EIA) during low solar activity, in CP, Brazil. Yokohama et
70 al. (2011) studied unusual patterns of echoes from coherent scatter radar data occurring
71 around midnight during the solar minimum period. They observed two principal types of
72 irregularities: the upwelling plumes and MSTID-like striations. They have argued that the
73 former can be generated by both the RT instability (at equatorial region) or to Perkins
74 instability (at mid-latitude region) and the later only by the Perkins instability. Yizengaw et
75 al. (2013) presented the study of the PMIs over equatorial Africa, and also investigated their
76 most probable causes. Dao et al. (2017) reported in a very interesting work the occurrence of
77 postmidnight field-aligned irregularities (FAIs) in Indonesia during low solar activity in
78 2010.

79 Many instrumental techniques are currently providing high-quality measurements and
80 results for ionospheric studies. Early investigations of the ionosphere referred to the diffuse
81 echoes seen in data from measurements using ionosondes, which are high-frequency radars
82 used for ionospheric sounding (Breit and Tuve, 1926; Booker and Wells, 1938). The



83 “spread-F” is widely used to generically refer to the irregularities observed in the equatorial
84 and low-latitude regions. Nowadays, digital ionosondes are extensively used for ground-
85 based sounding of the ionosphere, providing information from the E-region to the peak of
86 the F-layer, over a variable range of frequencies as well as features related to the
87 propagation of the irregularities (Reinisch et al., 2004; Batista et al., 2008, Abdu et al.,
88 2009). Equatorial spread-F has been extensively studied for several decades, and it is known
89 to be associated with the occurrence of large-scale plasma irregularities or equatorial plasma
90 bubbles (EPBs).

91 Optical imaging of thermospheric emissions, like that used in this work, is also a useful
92 ground-based technique for studying thermosphere/ionosphere processes. All-sky imaging
93 systems provide images of thermospheric emissions (e.g., OI 630-nm, OI 777.4-nm
94 emissions) at ionospheric heights over a large horizontal extent. The OI 630-nm emission
95 comes from recombination processes between molecular oxygen and electrons and presents
96 a volumetric emission rate which peaks at an altitude of ~250 km, around the F-layer the
97 bottom side height. In this way, variations in the intensity of the emission (dark and bright
98 regions) are used as tracers of ionospheric irregularities, such as EPBs, or other
99 disturbances, such as travelling ionospheric disturbances - TIDs (Pimenta et al., 2008;
100 Abalde et al., 2009; Makela et al., 2010; Candido et al., 2011; Chapagain et al., 2012).

101 For clarity for the present study, which presents a distinct pattern of spread-F from those
102 usually observed in equatorial ionograms, we first address the current state of understanding
103 regarding spread-F signatures in ionosonde data.

104 It is currently accepted that there are two main spread-F types: range and frequency type
105 spread-F traces (Abdu et al., 1998). The range type spread-F, often associated with the
106 occurrence of medium and large-scale irregularities, including EPBs, is comprised of trace
107 patterns with the echoes spread in range and with the onset beginning at the lower frequency



108 end of the F-layer trace in ionograms. During the spread-F season in Brazil, between
109 October and March, the evening pre-reversal enhancement in the zonal electric field, and
110 therefore the F-layer vertical drift, attains large values and range type spread-F is observed
111 in equatorial ionograms, followed by their appearance at crest region of the EIA, which is
112 located around Cachoeira Paulista (CP: 22.4° S, 45° W, dip angle: -37°). During the
113 remaining part of the year, when the vertical drifts are very small (Batista et al., 1996),
114 spread-F is restricted to the height region below the F-layer peak, rarely reaching the topside
115 ionosphere, and therefore observed only close to the dip equator. This type of spread-F is
116 usually classified as bottom side spread-F (Valadares et al., 1983). The other common
117 spread-F pattern observed in equatorial ionograms is the frequency type spread-F. In this
118 case, the spread-F echoes are seen at frequencies around the F-layer critical frequency
119 (foF2). It is believed to be associated with smaller scale/decaying irregularities following
120 spread-F/EPBs (Abdu et al., 1981a).

121 Some studies have pointed out that frequency type spread-F can sometimes be associated
122 with patches of ionization propagating eastward (MacDougall et al., 1998) and this type is
123 frequently observed in solstices in distinct longitudinal sectors. Additionally, both frequency
124 and range spread-F types can appear simultaneously, as a mixed spread-F pattern.

125 In this work, we present a case study on an unusual/anomalous spread-F/plasma
126 irregularities/depletions pattern observed over the equatorial region. We use the term
127 “unusual” in the sense that the observed features are distinct from those typically observed
128 for spread-F associated with post-sunset spread-F, as described above. Although the unusual
129 type of spread-F has been recognized since the early studies of the equatorial ionosphere
130 (Munro and Heisler, 1956; Heisler, 1958; Calvert and Cohen, 1961; Bowman, 2001), this is
131 the first time that it is reported for the Brazilian equatorial region with simultaneous airglow
132 observations, which reveal important ionospheric characteristics not available when using



133 only ionosonde data. The earlier studies extensively reported the occurrence of anomalies in
134 F-layer traces, such as cusps, F2 forking, and their possible association with TIDs. Calvert
135 and Cohen (1961) presented a comprehensive study of the distinct spread-F patterns. They
136 concluded that the distinct configurations or shapes of spread-F were associated with the
137 scattering in the vertical, east-west plane from field-aligned irregularities and that the
138 spread-F pattern depends on the position relative to the ionosonde and the scale sizes of the
139 irregularities.

140

141 **2. Data and Method**

142

143 **2.1 Digisondes**

144

145 We analyzed ionograms from two Digisondes DPS-4 operated at two Brazilian equatorial
146 sites: SL (44.2° W, 2.33° S, dip angle: -6.9°) and FZ (38.45° W, 3.9° S, dip angle: -16°),
147 which are separated in the east-west direction by ~ 600 km. Both instruments provided
148 ionograms at a 10-minute cadence. The DPS-4 also performs echo directional studies based
149 on Doppler interferometry, which provides information about the drift velocities associated
150 with irregularities. The operation of each Digisonde is based on the transmission of pulses at
151 digital frequencies from 1 to 20 MHz that are reflected from the ionosphere at plasma
152 frequencies lower than foF2. The maximum height range of the ionograms can be set at
153 ~ 700 or ~ 1400 km, for which the resolution is ~ 5 km and ~ 10 km, respectively. The
154 ionospheric true heights are calculated by an inversion method implemented by the ARTIST
155 software (Reinisch et al., 2005). Manual scaling of the data can be performed by editing the
156 ionograms using the SAO Explorer software (Galkin et al., 2008). The interferometry
157 system used by the Digisondes receiver is comprised of four small spaced antennas for



158 signal reception arranged in a triangle with one antenna at the center. The signals from each
159 antenna are Fourier analyzed to identify echoes with different Doppler frequencies (for more
160 details see Reinisch et al., 2004). The Drift Explorer software determines the location of the
161 source regions of the spread-F echoes for each Doppler component. The ionograms present a
162 color code showing the direction of echoes that form the spread-F. The sky map and drift
163 data collected after the ionogram are derived from the measured Doppler frequency and
164 angle of arrival of reflected echoes. Special processing software enables us to plot skymaps
165 showing the location of all reflection sources. The Drift Explorer also provides plots of the
166 drift velocities (zonal, vertical, and meridional components). For more details about
167 Digisondes sounding modes and drift measurements see Reinisch et al. (2005) and
168 references therein.

169

170 **2.2 Wide-Angle Imaging System**

171 The airglow images of the OI 630-nm emission used in this study were measured by a
172 Portable Ionospheric Camera and Small-Scale Observatory (PICASSO) wide-angle imaging
173 system deployed at Cajazeiras (CZ: 6.87° S, 38.56° W, dip angle: -21.4°), located about
174 ~352 km from south of FZ. It is a miniaturized imaging system that measures the 630.0-nm
175 and 777.4-nm nightglow emissions. Since the 777.4-nm emission is generally very weak
176 during solar minimum conditions, we use only the 630.0-nm emission image data for this
177 study. The PICASSO images are captured on a 1024 × 1024 Andor DU434 CCD with a
178 spatial resolution of approximately 1 km (azimuthal) over the entire field of view. The
179 spatial resolution in the radial direction varies from ~1 km to ~5 km from zenith to the edge
180 of the field of view. The noise contributions from dark current are reduced by cooling the
181 CCD to at least -60°C. The exposure time for each image is 90 s, and dark images are taken



182 frequently to remove noise and read-out biases. For details about the data processing from a
183 similar PICASSO installation, see Makela and Miller (2008).

184 **2.3 Fabry-Perot Interferometer (FPI)**

185

186 FPIs are optical instruments which measure the spectral line shape of the 630.0 nm emission
187 at around 250 km of altitude and are very useful to study thermospheric winds from Doppler
188 shifts in the emission's frequency. For more details of the FPI technique, see Fisher et al.,
189 (2015) and references therein. The investigation of the departures of the background wind
190 system can be useful to explain possible sources of the F-uplifts associated with late time RT
191 instability. For this purpose, we analyzed the behavior of the neutral winds over the
192 equatorial region taken from a ground-based FPI installed in CZ.

193

194 **3 Observations**

195

196 **3.1 Spread-F, F-layer height and plasma densities**

197

198 We present a case study of a spread-F event which occurred in the June solstice of 2011
199 during a geomagnetically quiet ($\Sigma Kp = 11$) night an low solar activity with mean $F10.7 = 97$
200 SFU (SFU is Solar Flux Unit = $10^{-22} \text{ W.m}^{-2}.\text{Hz}^{-1}$). Fig. 1 shows a sequence of ionograms on
201 26 July 2011 from 00:40 LT to 03:10 LT over SL (top panel) and over FZ low latitude site
202 (bottom panel) from 25 July 2011 at 22:00 LT to 26 July 2011 01:30 LT in which the
203 presence of unusual spread-F patterns is observed. Over SL, the first spread-F trace appears
204 at 01:00 LT at an oblique angle close to or above the F-layer peak at a virtual range of 600
205 km. Over the next hour, this structure gradually moves closer to the station SL, finally
206 merging with F-layer bottom side echoes and becoming a well-formed spread-F trace.



207 During the spread-F development, it is possible to observe an apparent small increase in the
208 F-layer heights. Finally, at the end of the spread-F event, around 02:50 LT, we observe a
209 decreased foF2 and the formation of an Es layer, lasting until 03:10 LT (not shown). We
210 notice a very similar evolutionary pattern of the structures in the FZ ionograms as in those
211 obtained from SL. However, the first spread-F traces appeared over FZ around 22:20 LT,
212 much earlier than over the equatorial site, SL. These echoes from FZ lasted for about 3
213 hours. The spread-F echoes gradually move closer to the station or downward to form a
214 well-structured spread-F pattern.

215 An important point to be considered is the local ionospheric background in which the
216 spread-F occurred. The F-layer parameters, h'F (virtual height of the F-layer bottom side, in
217 km), the hmF2 (the real height of the F-layer peak, in km) and foF2 (the F-layer critical
218 frequency, in MHz) for both stations are shown in Fig. 2 from 18:00 LT to 06:00 LT. Over
219 SL an uplift of the F-layer was observed between 21:00 LT and 23:00 LT, not associated
220 with any spread-F echoes. Near 21:00 LT we may note some wave-like oscillations in the F-
221 layer height (notable in hmF2) (with a period on the order of one hour. The first spread-F
222 trace at oblique angles (and perhaps above the F2 peak) appeared during these oscillations.

223 On the other hand, over FZ where heights are lower, we observe stronger wave-like
224 oscillations in both h'F and hmF2 three hours earlier than observed at SL. The F-layer
225 critical frequency decreased for both stations, as it is expected for this period. At the
226 beginning of the spread-F occurrence, the foF2 was as low as 4 MHz, corresponding to an
227 electron density of 1.98×10^5 el.cm⁻³. The parameter fxI (not shown), or top frequency of
228 spread-F, which is the highest frequency of spread-F echoes, reached values not higher than
229 4.5 MHz over SL but reached values around 6.0 MHz over FZ, which means higher plasma
230 density at this region. Moreover, after the spread-F ceased, it was possible to observe the
231 recovery of the plasma frequency/density over FZ sooner than over SL.



232

233

234 **3.2 Depletions in the airglow OI 630.0-nm emission**

235

236 Figure 3 shows a sequence of four images of the OI 630.0-nm emission collected on 25-26
237 July 2011 at Cajazeiras (CZ: center of the frame), Brazil. The images are projected over a
238 geographic map of Brazil assuming an emission altitude of 250 km. The sites of FZ and SL
239 are also indicated in the top-left panel. Between 23:12 LT to 01:26 LT at least two
240 depletions can be observed propagating westward. These depletions passed over FZ and CZ
241 at 23:12 LT, in agreement with the spread-F traces seen in the ionograms from FZ.

242

243 **3.3 F-layer irregularity Drifts – Directions and Velocities**

244 Automatic drift mode routines were used to obtain information about the location of echo
245 sources in the F-layer associated with plasma irregularities. These routines provide
246 information about the distance of the reflected echoes, using measurements of the radar
247 ranges to the vertical and oblique echoes as well as their directions, as described by Reinisch
248 et al. (2004). The distribution of the echoes can be displayed in skymaps as shown in Fig. 4.
249 Skymaps between 00:12 LT and 00:42 LT were constructed using data from FZ during the
250 spread-F event studied where reflected echoes appear and are distributed in a west-east
251 elongated pattern covering a total horizontal distance of 1200 km (from west to east). It may
252 be noted that, in general, negative Doppler velocity (yellow color) of the echoes dominates
253 the western azimuth while the eastern azimuth is dominated by positive Doppler velocity
254 (blue color), a characteristic that is indicative of an overall westward motion of the
255 irregularity structures. Additional directional information is obtained from the temporal
256 evolution of each spread-F echo in plots of the horizontal distance of the echoes (horizontal



257 axis) as a function of time (vertical axis), presented as directograms. A directogram for the
258 night of 25-26 July 2011 constructed using data from FZ is shown in Fig. 5. Each horizontal
259 line of the directogram corresponds to a single ionogram. The spread echoes are distributed
260 east to west from 21:00 LT to ~ 05:00 LT, although there is only a sparse distribution
261 between 21:00 and 23:00 LT. The color codes at both sides indicate the incoming and
262 outgoing direction of the reflectors (irregularities), while the arrow indicates the direction of
263 propagation. For example, some echoes are seen at ~415-km east around 23:30 LT. The
264 color code indicates they are at east of the station coming from the east side. Also, there are
265 echoes at the east of the station which come from northeast, NNE, direction. Among these
266 echoes, there are only a few points that are going eastward (blue points). From 23:30 to
267 01:30 LT, there are echoes at west which gradually disappear after 02:00 LT. The color code
268 to the left shows that they are at west from the station and going westward. Thus, the echoes
269 present a mean westward propagation. We point out that the horizontal distance range limit
270 is around 600 km, which correspond to an antenna beam angle of approximately 45° , as it is
271 seen in the directograms on Fig. 5, and h_{min} is the spread-F reflection height.

272 The unusual spread-F echoes were observed at both equatorial sites, SL and FZ, with a zonal
273 separation of ~600 km. The first spread-F trace was observed at 22:20 LT over FZ and later
274 at 01:00 LT over SL. This lag of ~ 02:40 hours suggests an average westward drift velocity
275 component of $\sim 62 \text{ ms}^{-1}$. The DPS-4 drift mode provides the full-vector Doppler velocity for
276 the observed echoes. Figure 6 shows the variation of the V_z (vertical component) and V_{east}
277 (zonal component) velocities taken from measurements of the Digisonde DPS-4 (drift mode)
278 from 21:00 LT on July 25, 2011, to 04:00 LT on July 26, 2011. Positive (negative) V_{east}
279 velocities represent eastward (westward) propagation. $|V|$ represents the zonal drift Doppler
280 velocities are less than 50 ms^{-1} , while the maximum vertical upward component is $\sim 40 \text{ ms}^{-1}$.
281 The zonal velocities inferred from Drift Explorer agree well with the estimate obtained from



282 the difference in onset times of spread-F echoes between SL and FZ, with a mean value of
283 $\sim 55 \text{ ms}^{-1}$ during the event. The middle panel is the vector diagram with the variations of the
284 mean total electrodynamical drift velocity (see Balan et al., 1992). For clarity, the vector
285 length is fixed, and the information on $|V|$ is represented by the circles (arrow start point).
286 As it is observed, the vector is found to rotate anticlockwise, starting in the east-up sector in
287 the night and reaching west-up sector in post-midnight. Velocities extracted from the
288 airglow images obtained from CZ are shown in the bottom panel of Fig. 6. To estimate the
289 velocity of the depletion structure, the individual images were processed by first spatially
290 registering the 630.0-nm images using the star field. After removing the stars from the
291 images using a point suppression methodology, the images were projected onto geographic
292 coordinates assuming an airglow emission altitude of 250 km (for details of analysis
293 technique see Chapagain et al., 2012). The depletion structure was selected in consecutive
294 images to find the zonal shift of the structures from which the velocity was estimated. The
295 estimated zonal propagation velocity was $\sim 60 \text{ ms}^{-1}$, which agrees well with the velocities
296 determined by the Doppler technique of the Digisonde. We should keep in mind that the
297 Digisonde Doppler technique determines the mean irregularity motion while the velocities
298 from the airglow technique estimate the mean propagation of the plasma depletion.

299 Figure 7 presents the variation of F-layer height (fixed frequencies) in both stations,
300 SL and FZ. This plot can be useful to analyze the oscillations in the F-layer bottom side and
301 the possible association with gravity waves.

302

303 **3.4 Thermospheric Winds**

304 Figure 8 shows the measured thermospheric zonal (top panel) and meridional (bottom panel)
305 wind on July 25-26, taken from the FPI installed in CZ, the same location where the airglow
306 images were obtained. The shaded region is the standard deviation of the monthly average,



307 the green lines are the average winds on July 25-26 (± 2 days), and the red line is the
308 measurement for July 25-26. It is observed that on July 25-26 between 22:00 LT and 01:00
309 LT the zonal wind is abnormally eastward (~ 100 m/s), while the meridional wind departs
310 from the monthly and daily variation average. Additionally, it is observed an equatorward
311 wind (~ 30 m/s). From this, we can consider that a possible balance between the zonal and
312 meridional wind component may be responsible by plasma advection (plasma movement)
313 from low latitude to equatorial region, which might have maintained the F-layer at a higher
314 altitude as discussed by Nicolls et al., 2006. This apparent uplifts observed in both stations
315 around 00:00 LT might have caused the development of late RT-instability and the PMIs.

316

317 **4 Discussion**

318

319 We present an unusual event of PMIs/spread-F/depletions over the equatorial site in Brazil
320 that exhibits singular features. This is the first report of such distinct type of spread-F for the
321 Brazilian equatorial region, though it was observed earlier at the low latitude station CP
322 (Brazil) for the solar minimum 2008-2009 by Candido et al., 2011. A careful analysis of
323 equatorial ionograms and other plots from digisonde soundings suggest modifications in the
324 ionospheric plasma density structuring, such as those associated with plasma density
325 depletions, which are responsible for a variety of spread F-layer patterns.

326

327 **4.1 Depletions in the airglow OI 630.0 nm images**

328

329 Airglow images show an apparent southwestward propagation of depletions on this night,
330 which differs from the typical propagation direction of post-sunsets EPBs. However, this
331 atypical propagation can be a characteristic of post-midnight depletions and needs further



332 investigation with a long-term airglow database. The depletions also propagated over CZ
333 (350 km south of FZ) with mean westward velocities $\sim 60 \text{ ms}^{-1}$ which are similar to the
334 velocities of propagation of the irregularities observed with the Digisonde at FZ. Some
335 authors have demonstrated that EPBs can also present westward propagation after midnight
336 during quiet times (Paulino et al., 2010; Sobral et al., 2011). However, they defined in those
337 studies that the depletions associated with EPBs should first present movement to the east
338 earlier in the evening and reversal to westward at later hours. This is not the case for the
339 structures presented in this work since there are no depletions in the OI 630.0-nm images
340 propagating eastward earlier in the evening.

341 Moreover, Sobral et al. (2011), interpreted that westward traveling plasma bubbles (WTPB)
342 observed at the same region were associated with westward zonal thermospheric winds
343 (simulated results). On the other hand, Fisher et al. (2015) presented a climatological study
344 of the quiet time thermospheric winds and temperatures by measurements of the OI 630.0
345 nm airglow emission spectral line shape over the same region. They noticed that during low
346 solar activity ($F_{10.7} < 125 \text{ sfu}$), the zonal and meridional winds are, on average, negligible
347 in postmidnight hours. It is possible that these differences can be attributed to departures
348 from the wind system at which could be responsible by the F-layer uplifts and plasma
349 instabilities/irregularities development.

350

351 **4.2 Spread-F in ionograms**

352 As mentioned before, spread-F echoes in ionograms generally appear first at the low-
353 frequency end, as satellite traces, evolving into spread-F echoes extended in frequency and
354 range. These characteristics were not seen in the present study. In this work, the reflected
355 echoes observed in the ionograms first came from oblique directions and at heights which
356 could be considered possibly higher than those observed overhead. The spread echoes



357 appear at the higher frequency edge of the F-layer, with top-frequency higher than the layer
358 critical frequency. Subsequently, the low-frequency edge of the cusp merges with the main
359 trace, while the baseline of the spread-F traces gradually decreases in height. Anomalous
360 traces in F-layer ionograms, such as ‘cusps’ or ‘spurs,’ were described in earlier studies to
361 be associated with traveling disturbances in the ionosphere. Munro and Heisler (1956) and
362 Heisler (1958) have observed the occurrence of anomalous traces in ionograms and
363 attributed them to the manifestations of TIDs. As it is well known, TIDs can be described as
364 frontal gravity waves propagating horizontally in the ionosphere, causing increases and
365 decreases in the ionization, i.e., horizontal gradients in the ionization. According to Munro
366 and Heisler (1956), changes in the ionization would be responsible for the anomalous traces
367 in the F-layer ionogram. Similar occurrences were reported by Ratcliffe (1951) for
368 ionograms from Huancayo, Peru. Calvert and Cohen (1961) have pointed out that some
369 spread-F traces observed over Huancayo presented characteristics similar to frequency
370 spread-F from “temperate” latitudes, which are mainly associated with TIDs. Also, they
371 studied distinct configurations of spread-F with echoes coming from oblique directions,
372 similar to what is presented in this work. The oblique echoes observed in ionograms alone
373 could not provide their zonal direction (from east or west). However, additional directional
374 information provided from the drift mode sounding of the Digisonde DPS-4 and their
375 appearance first in the ionograms over FZ followed by their occurrence over SL (a western
376 site in relation to FZ), suggested that they propagated westward. Late/pre-dawn spread-F
377 was also reported by McDougall et al. (1998) for solstices in the Brazilian sector. However,
378 they considered the occurrence of late time spread-F during December solstice at Fortaleza
379 as patches of ionization, which cause spread echoes at the high-frequency end or the
380 frequency spread-F. They also concluded that the echoes did not come from overhead
381 structures but from the east or west directions.



382 **4.3 Post-midnight irregularities/F-region background conditions**

383

384 As it is well-known, the poor alignment between the sunset terminator and the magnetic
385 field lines during June solstice in Brazil is responsible by the low occurrence rate of post-
386 sunset spread-F/EPBs, since the vertical plasma drifts are very weak. However, it is
387 observed a secondary occurrence peak of spread-F/plasma irregularities in June solstice
388 during late night, especially in post-midnight. For this, it is necessary to have an F-layer
389 uplift, which creates favorable conditions for the development of the RT instability. These
390 conditions are not completely understood, and they have been discussing by several authors
391 (McDougall et al., 1998; Nicolls et al., 2006; Abdu et al., 2009; Nishioka et al., 2012,
392 Yokohama et al., 2012, Ajith et al., 2016).

393 During the high solar activity, the longitudinal variation of the declination angle is
394 predominant on the F-layer vertical drift and the occurrence of the plasma irregularities,
395 while it is not important during solar minimum. During low solar activity/solar minimum, in
396 the absence of geomagnetic disturbances, the seeding processes related to gravity waves
397 seem to be more important, especially when the PRE-amplitude is small or absent
398 (Balachandran et al., 1992; Abdu et al., 2009). In this way, we should address the conditions
399 which precede the occurrence of the post-midnight irregularities observed in this work. It is
400 noticed that spread-F traces associated with plasma irregularities were detected firstly at
401 oblique directions at least 500 km at east or west from the station, as seen in the
402 directograms in Figure 5, which we can consider as ionospheric conditions favorable in a
403 wide longitudinal range.

404

405

406



407 **4.3.1 Thermospheric winds**

408

409 Nicolls et al. (2006) discussed the nocturnal F-layer uplifts associated with the
410 secondary maximum of spread-F occurrence rate in low solar activity. As it is well
411 understood, the nocturnal westward electric field is responsible by the downward movement
412 of the F-layer. During solar minimum, these electric fields can be easily reversed by a weak
413 geomagnetic disturbance. However, in the absence of the geomagnetic disturbance, which is
414 the case studied in this work, other sources should be considered. Analyzing F-layer uplifts
415 for different conditions of solar activity, Nicolls et al. (2006) verified that during downward
416 F-layer movement (decreasing westward electric field), even a small contribution of a
417 meridional equatorward wind (~30m/s), could lead the F-layer to higher heights triggering
418 the RT instability.

419 Moreover, it was discussed that neutral winds could not uplift the equatorial plasma directly,
420 but they are sources of meridional advection (movement) of plasma, driven by a latitudinal
421 gradient in electron density, responsible by F-layer uplifts. They concluded that the uplifts
422 could be due to the decreasing, not to the reversal, of the westward zonal electric field
423 associated with departures in the wind system related to the midnight temperature maximum
424 (MTM), recombination processes, and the plasma flux. In this way, we analyze the zonal
425 and the meridional neutral wind variation in Figure 8, in order to verify that there are
426 suitable conditions for F-layer uplift. As it is observed in Figure 8 (top panel), the zonal
427 wind is ~100 m/s just before midnight while meridional wind (equatorward) is ~30 m/s just
428 after midnight (bottom panel). There is evidence that the mean equatorward meridional
429 winds have kept the F-layer at higher altitudes enough to the trigger the RT instability
430 development.

431



432

433 **4.3.2 Recombination processes - Rayleigh Taylor instability growth rate**

434 Nishioka et al. (2012) discussed the causes of the postmidnight uplifts that occurred during
435 winter in Chumphon, Thailand (low latitude) and the post-midnight Field-Aligned
436 Irregularities, FAIs, in Kototaband, Indonesia (equatorial region). As it is well known, the
437 zonal electric field is westward during the night, as the vertical drift \mathbf{ExB} is downward. This
438 condition leads to an RT-instability growth rate negative. In this way, it is important to
439 address, the importance of the term g/v_{in} in the linear growth rate of RT-instability, and of
440 the recombination processes, as shown in Equation (1):

$$441 \quad \gamma = \left(\frac{E}{B} + \frac{g}{v_{in}} \right) \frac{1}{L} \quad (1)$$

442 Where: E is an the electric field; B is the magnetic field; g is gravity acceleration, v_{in} is ion-
443 neutral collision frequency; L is the scale length of the vertical gradient of the F-region
444 plasma density. At night, the zonal electric field is westward, as the growth rate can be
445 negative, i.e., the F-layer bottom side is stable. On the other hand, the term g/v_{in} may hands
446 out in the following conditions: 1) v_{in} is proportional to the neutral density, n , where n is
447 smaller during the night than the day; 2) v_{in} is smaller at higher altitudes owing to the
448 decrease of n with the height; 3) v_{in} is smaller during low solar activities. Therefore, under
449 the appropriate conditions, the RT growth rate can be positive, although small, as it is
450 observed in this work. To understand the recombination processes as a source of the F-layer
451 uplift it should be considered that the F-layer bottom side is eroded if it is at lower altitudes
452 (at ~300 km), such as there is a decreasing of peak density and the increasing of F-layer
453 peak height. For clarity, we present the F-layer density profiles, in Fig. 9, taken from
454 measurements using the Digisonde installed in SL. It is possible to observe that from 22:00
455 to 00:00 LT, the F-layer peak height, and peak density decrease. As the F-layer bottom side



456 is at a lower height, it is observed an apparent F-layer uplift, which can be attributed to the
457 recombination process at the bottom side.

458

459 **4.3.3 Es-layer electric fields**

460

461 The role of Es-layer has been considered as a possible cause for the late-time RT instability
462 development. Low latitude Es-layer can provide enough polarization electric field which
463 maps to equatorial F-layer bottom side, causing F-layer uplift, as pointed out by Yizengaw
464 et al. (2013). They interpreted the occurrence of late plasma irregularities/EPBs over Africa
465 coast during the same period of this work, June solstice 2011, and discussed that during
466 quiet geomagnetic nights, there were favorable conditions for the action of polarization
467 electric fields associated with low latitude Es layer/instability which mapped to the
468 equatorial F-layer along the geomagnetic field lines seeding RT-instability and irregularities.
469 In fact, in this work, we can observe the occurrence of the Es-layer at the both quasi-
470 equatorial station FZ and at SL, at around 00:00 and 02:50 LT respectively. However, the
471 influence of Es-layers on late time F-layer uplift in this work is not clear since they occur at
472 the same location of the spread-F. Its influence on the post-midnight spread-F during solar
473 minimum is worth of investigation in further works.

474

475 **4.3.4 Mesoscale Travelling Ionospheric Disturbances, MSTIDs and Gravity-Waves,** 476 **GW**

477 MSTIDs have been reported in Brazilian low latitudes using airglow and ionosonde
478 (Candido et al., 2008, 2011; Pimenta et al., 2008). They appear as large-scale dark bands
479 aligned from northeast to southwest propagating northwestward mainly during low solar
480 activity and are associated with electrodynamic forces in mid-latitudes (Perkins instability)



481 or by the propagation of gravity waves in ionospheric heights at low latitudes or equatorial
482 region. If they propagate at equatorial ionospheric heights, they can be seen as oscillations in
483 the F-layer bottom side and can trigger RT-instability and plasma bubbles. In this work, the
484 plasma irregularities seen by the ionosonde are preceded by small oscillations in the F-layer
485 bottom ($h'F$) and peak heights ($hmF2$). However, oscillations are usually observed in the F-
486 layer bottom side, and it should be carefully considered in order to establish if they are
487 associated with GWs. Generally, they are considered associated with GW if it downward
488 phase propagation is observed in the fixed frequencies (isolines) plots, i.e., the oscillations
489 are seen firstly in the higher frequencies. Figure 7 showed the occurrence of oscillations in
490 F-layer through some fixed frequencies (isolines) in both stations FZ and SL, although the
491 downward propagation is not exactly clear. On the other hand, the spread-F pattern observed
492 in this work is quite similar to those reported by Candido et al. (2011) during the descending
493 phase/solar minimum at low latitudes in CP. This feature could suggest that they could be
494 caused by low latitudes MSTIDs propagating equatorward or associated to the action of
495 polarization electric fields mapping from low latitudes MSTIDs structures to the equatorial
496 F-layer bottom side. This kind of event was reported by Miller et al. (2012), which studied
497 the occurrence of EPBs on the same night of the occurrence of MSTIDs propagating in mid-
498 latitudes and attributed them to the action of the electric field from these MSTIDs in the F-
499 layer region. However, the depletions observed in the OI 630-nm emission (Figure 3)
500 present distinct features (propagation direction) of those associated to MSTIDs coming from
501 low latitudes reported by Candido et al. (2011). Also, they are not similar to the depletions
502 associated with the typical EPBs which propagate eastward. Recent results by Takahashi et
503 al. (2018) reported the occurrence of equatorial MSTIDs in high solar activity conditions
504 (2014/15), which were associated with periodic plasma bubbles in the Total Electron



505 Content (TEC) maps in the same region. They showed evidence of tropospheric sources for
506 the development and propagation of GWs at ionospheric heights.

507 Finally, we should address that, as shown in Figs.2 and 7, late height rise (in both h'F and
508 hmF2) with smaller amplitude waves are observed at SL starting at ~ 21:00 LT when the
509 base height (h'F) increased to > 250 km. Such a condition can be suitable for the growth of
510 RT instability. Over FZ, a similar sequence of variations occurred starting at ~23:00 LT in
511 hmF2. Notice that h'F and hmF2 values were significantly smaller than those at SL.

512 However, it is notable that the oscillations in the F layer heights, especially in hmF2, (with
513 the period around 36 min) that preceded the spread F traces (at both sites) are significantly
514 higher in amplitude at FZ than at SL. This aspect can be noted in more detail in the iso-line
515 plots of plasma frequencies presented in Fig. 7, where in the height oscillations show larger
516 amplitude and occurring at earlier local times than they are at SL. Such oscillations may be
517 associated with gravity waves propagating to ionospheric heights with preferential
518 propagating directions to northeast and southeast, as recently reported by Paulino et al.
519 (2016). These oscillations are indicative of the seed perturbations to lead to the SF
520 irregularity development through RT mechanism. Depending upon the amplitude of the seed
521 perturbation, even the small increases in the F layer height that marked this period, could be
522 capable of seeding RT instability and consequently generate the spread F irregularities (see,
523 for example, Abdu et al., 2009). To explain the non-local origin of the SF traces, as observed
524 at both sites, it will be necessary to assume that the precursor conditions that existed at SL
525 and FZ must have continued to exist in longitude extending further eastward of Fortaleza,
526 perhaps with some increase in intensity so that the irregularities generated therein and
527 drifting westward could be the origin of the oblique spread F trace first observed over FZ
528 and later over SL.



529 It is plausible to consider that the depletions observed in this work can be associated with
530 atypical EPBs triggered by GWs/MSTIDs at locations at the east of FZ and SL or to F-layer
531 uplifts caused by departures from wind system simultaneously to a weakening of the
532 westward zonal electric field (not shown here) during low solar activity. We should notice
533 that the observational techniques used in this work are complementary and validate each
534 other to identify “anomalous” spread-F patterns associated with plasma
535 irregularities/depletions and can help the understanding of the ionosphere during low solar
536 activity. The drift mode is very useful and suitable for tracking plasma irregularities and
537 their evolution in the absence of other techniques.

538

539 **5 Summary and Conclusions**

540 In this paper, we have presented and discussed an unusual spread-F pattern associated with
541 unusual depletions on the OI 630.nm airglow emission observed during geomagnetically
542 quiet conditions during the June solstice of 2011 over the equatorial region in Brazil. We
543 summarize our findings as:

- 544 1) The unusual spread-F pattern studied in this work present a distinct feature from those
545 usually observed at post-sunset hours;
- 546 2) The spread-F/depletions occurred during low plasma density conditions, geomagnetically
547 quiet nights, low solar activity and propagated westward.
- 548 3) The processes to generate spread-F at equatorial latitudes during quiet time seems to be
549 associated with the late time F-layer uplifts, possibly caused by departures in the neutral
550 wind system, probably associated with a weakening of the westward electric field, or to the
551 propagation of GWs at ionospheric heights, which favor the development of the late-time
552 RT-instability.



553 4) The spread-F event discussed here presents characteristics similar to those of the earlier
554 cases reported for low latitudes in CP during June solstice of solar minimum 2008-2009 by
555 Candido et al., 2011.

556

557 The instrumental approach in this work seems to be suitable for further ionospheric studies,
558 modeling, and forecast during low solar activity.

559

560

561 **Abbreviations**

562

563 SL: Sao Luis

564 FZ: Fortaleza

565 CZ: Cajazeira

566 CP: Cachoeira Paulista

567 DPS: Digital portable sounder

568 FPI: Fabry-Perot Interferometer

569 EPBs: Equatorial plasma bubbles

570 PMIs: Postmidnight plasma irregularities

571 RT: Rayleigh-Taylor

572 EIA: Equatorial ionization anomaly

573 MSTIDs: Meso-scale traveling ionospheric disturbances

574 FAIs: Field-aligned irregularities

575 TIDs: Travelling ionospheric disturbances

576 SFU: solar flux unity

577 LT: local time

578 UT: Universal time



579 MTM: midnight temperature maximum

580 GWs: Gravity waves

581

582 **Data availability**

583 The processed data used in this work can be requested to the author CMNC by the email:

584 claudia.candido@inpe.br. The raw data: Digisonde data is available in the website:

585 www.inpe.br/embrace. The airglow and Fabry-Perot data should be requested to the author:

586 JM, by the email: jmakela@illinois.edu.

587

588 **Author Contributions**

589 CMNC wrote the manuscript and plotted the graphics of the ionospheric parameters. FBG

590 helped with part of the graphics and revised the manuscript. JS, ISB, EC, MAA, N.B., ZL,

591 CW read and made suggestions to the manuscript. JM and NC provided the airglow figures

592 and Fabry-Perot data and plots, as well as read the manuscript and suggested corrections. All

593 the authors read, give comments and suggestions to the work and agree with the content and

594 submission of this manuscript.

595

596 **Competing interests**

597 The authors declare they have no conflicts of interest.

598

599 **Acknowledgments**

600 C.M.N.C thanks the Brazilian funding agency CNPq for the financial support through the

601 process n.64537/2015-5, and to China-Brazil Joint Laboratory for Space Weather and the

602 National Natural Science Foundation of China for the project with No.41474137 and

603 1674145 for the postdoctoral fellowship. Also, we thank INPE technical staff for the

604 assistance with the instrumentation and data management. N.P.C. was supported by the

605 NASA Living With a Star Heliophysics Postdoctoral Fellowship Program, administered by



606 the University Corporation for Atmospheric Research (UCAR). Work at the University of
607 Illinois at Urbana-Champaign was supported by National Science Foundation CEDAR grant
608 AGS 09-40253 and was performed in collaboration with J. W. Meriwether at Clemson
609 University. We are grateful to the Universidade Federal de Campina Grande and Dr. Ricardo
610 A. Buriti for the support to the imaging systems installed at Cajazeiras.

611

612 **6 References**

613

614 Abalde, J. R., Sahai, Y., Fagundes, P. R., Becker-Guedes, F., Bittencourt, J. A., Pillat, V.
615 G., Lima, W. L. C., Candido, C. M. N., and de Freitas, T. F.: Day-to-day variability in the
616 development of plasma bubbles associated with geomagnetic disturbances, *J. Geophys. Res.*,
617 114, A04304, doi:10.1029/2008JA013788, 2009.

618

619 Abdu, M. A., Bittencourt, J. A., Batista, I. S.: Magnetic declination control of the equatorial
620 F region dynamo field development and spread F, *J. Geophys. Res.*, v. 86, p. 11443-11446,
621 1981a.

622

623 Abdu, M. A., Batista, I. S., and Bittencourt, J. A.: Some characteristics of spread F at the
624 magnetic equatorial station Fortaleza, *J. Geophys. Res.*, 86, A8, 6836-6842, 1981b.

625

626 Abdu, M. A., Batista, I. S., Kantor, I. J., Sobral, J. H. A.: Gravity-Wave Induced Ionization
627 Layers in the Night F-Region over Cachoeira Paulista (22° S, 45° W), *J. Atmos. Terr. Phys.*,
628 44 (9), 759-767, 1982.

629

630 Abdu, M. A., Batista, I. S., Reinisch, B. W., de Souza, J. R., Sobral, J. H. A., Pedersen, T.
631 R., Medeiros, A. F., Schuch, N. J., de Paula, E. R. and Groves, K. M.: Conjugate Point
632 Equatorial Experiment (COPEX) campaign in Brazil: Electrodynamics highlights on spread



- 633 F development conditions and day-to-day variability, *J. Geophys. Res.*, 114, A04308,
634 doi:10.1029/2008JA013749, 2009.
- 635
- 636 Balan, N.; Jayachandran, B.; Balachandran Nair, R.; Namboothiri, S. P.; Bailey, G. J.; Rao,
637 P. B.: HF Doppler observations of vector plasma drifts in the evening F-region at the
638 magnetic equator, *J. Atmos. Terr. Phys*, 54, (11/12), pp. 1545-1554, 1992.
- 639
- 640 Balachandran Nair, R., Balan, N., Bailey, G. J., and Rao, P. B.: Spectra of the ac electric
641 fields in the post-sunset F-region at the magnetic equator, *Planet. Space Sci.*, 40(5), 655–662.
642 [https://doi.org/10.1016/0032-0633\(92\)90006-A](https://doi.org/10.1016/0032-0633(92)90006-A), 1992.
- 643
- 644 Balan N., Liu, L. B., and Le, H. J.: A brief review of equatorial ionization anomaly and
645 ionospheric irregularities, *Earth Planet. Phys.*, 2(4), 1–19.
646 <http://doi.org/10.26464/epp2018025>, 2018.
- 647
- 648 Batista, I. S., de Medeiros, R. T., Abdu, M. A., de Souza, J. R.: Equatorial Ionospheric
649 Vertical Plasma Drift Model over the Brazilian Region, *J. Geophys. Res.*, 101 (A5), 10887-
650 10892, 1996, 1996.
- 651
- 652 Batista, I. S., and Abdu, M. A: Ionospheric variability at Brazilian low and equatorial
653 latitudes: Comparison between observations and IRI model, *Adv. Space Res.*, 34, 1894–
654 1900, doi:10.1016/j.asr.2004.04.012, 2004.
- 655
- 656 Batista, I. S., Abdu, M. A., Carrasco, A. J., Reinisch, B. W., Paula, E. R., Schuch, N. J.
657 and Bertoni, F.: Equatorial spread F and sporadic E-layer connections during the Brazilian



- 658 Conjugate Point Equatorial Experiment (COPEX), *J. Atmos. Sol. Terr. Phys.*, 70, 1133-1143,
659 doi:10.1016/j.jastp.2008.01.007, 2008.
- 660
- 661 Booker, H. G., and Wells, H. W.: Scattering of radio waves in the F-region of the ionosphere,
662 *Terr. Magn. Atmos. Electr.*, 43, 249–256, doi:10.1029/TE043i003p00249, 1938.
- 663
- 664 Bowman, G. G.: A comparison of nighttime TID characteristics between equatorial
665 ionospheric anomaly crest and midlatitude regions, related to Spread F occurrence, *J.*
666 *Geophys. Res.*, 106(A2), 1761–1769, doi: 10.1029/2000JA900123, 2001.
- 667
- 668 Breit, G. and Tuve, M. A.: A Test for the Existence of the Conducting Layer, *Phys. Rev.*, 28,
669 pp. 554-575; 1926.
- 670
- 671 Calvert, W., and Cohen, R.: Interpretation and Synthesis of Certain Spread-F Configurations
672 Appearing on Equatorial Ionograms, *J. Geophys. Res.*, 66 (10), 3125-32, 1961.
- 673
- 674 Candido, C. M. N., Pimenta, A. A., Bittencourt, J. A., Becker-Guedes, F.: Statistical analysis
675 of the occurrence of medium-scale traveling ionospheric disturbances over Brazilian low
676 latitudes using OI 630.0 nm emission all-sky images, *Geophys. Res. Lett.*, 35, L17105, doi:
677 10.1029/2008GL035043, 2008.
- 678
- 679 Candido, C. M. N., Batista, I. S., Becker-Guedes, F., Abdu, M. A., Sobral, J. H. A., and
680 Takahashi, H.: Spread F occurrence over a southern anomaly crest location in Brazil during
681 June solstice of solar minimum activity, *J. Geophys. Res.*, 116, A06316,
682 Doi:10.1029/2010JA016374, 2011.



683

684 Carter, B. A., Zhang, K., Norman, R., Kumar, V. V. and Kumar, S.: On the occurrence of
685 equatorial F-region irregularities during solar minimum using radio occultation
686 measurements, *J. Geophys. Res. Space Physics*, 118, 892–904, doi:10.1002/jgra.50089,
687 2013.

688

689 Chapagain, N. P., Makela, J. J., Meriwether, J. W., Fisher, D. J., Buriti, R. A. and Medeiros,
690 A. F.: Comparison of Nighttime Zonal Neutral Winds and Equatorial Plasma Bubble Drift
691 Velocities over Brazil, *J. Geophys. Res.*, doi: 10.1029/2012JA017620, 2012.

692

693 Dao, T., Y. Otsuka, Shiokawa, K., Tulasi Ram, S., and Yamamoto, M.: Altitude
694 development of postmidnight F region field-aligned irregularities observed using Equatorial
695 Atmosphere Radar in Indonesia, *Geophys. Res. Lett.*, 43, 1015–1022, doi:10.1002/
696 2015GL067432, 2016.

697

698 Galkin, I. A., Khmyrov, G. M., Reinisch, B. W., and McElroy, J.: The SAOXML 5: New
699 format for ionogram-derived data, in *Radio Sounding and Plasma Physics*, AIP Conf. Proc.
700 974, 160-166, 2008.

701

702 Heisler, L. H.: Anomalies in ionosonde records due to traveling ionospheric disturbances,
703 *Austr. J. Phys.*, V.11, pp. 79, 1958.

704

705 Li, G., Ning, B., Abdu, M. A., Yue, X., Liu, L. Wan, W., and Hu, L.: On the occurrence of
706 postmidnight equatorial F region irregularities during the June solstice, *J. Geophys. Res.*,
707 116, A04318, doi:10.1029/2010JA016056, 2011.



708

709 Liu, L., Yang, J., Le, H., Chen, Y., Wan, W., and Lee, C. C.: Comparative study of the
710 equatorial ionosphere over Jicamarca during recent two solar minima, *J. Geophys. Res.*, 117,
711 A01315, doi:10.1029/2011JA017215, 2012.

712

713 MacDougall, J. W.; Abdu, M.A., Jayachandran, P. T., Cecile, F., Batista, I. S.: Presunrise
714 spread F at Fortaleza, *J. Geophys. Res.*, 103 (A10), 23415-23425, 1998.

715

716 MacDougall, J., Abdu, M. A., Batista, I., Buriti, R., Medeiros, A. F., Jayachandran, P. T.,
717 and Borba, G.: Spaced transmitter measurements of medium-scale traveling ionospheric
718 disturbances near the equator, *Geophys. Res. Lett.*, 38, L16806,
719 Doi:10.1029/2011GL048598, 2011.

720

721 Makela, J. J., and Miller, E. S.: Optical observations of the growth and day-to-day variability
722 of equatorial plasma bubbles, *J. Geophys. Res.*, 113, A03307, doi:10.1029/2007JA012661,
723 2008.

724

725 Makela, J. J., Kelley, M. C., and Tsunoda, R. T.: Observations of midlatitude ionospheric
726 instabilities generating meter scale waves at the magnetic equator, *J. Geophys. Res.*, 114,
727 A01307, doi: 10.1029/ 2007JA012946, 2009.

728

729 Makela, J. J., Miller, E. S., Tallat, E.: Nighttime medium-scale traveling ionospheric
730 disturbances at low geomagnetic latitudes, *Geophys. Res. Lett.*, 37, L24104,
731 doi:10.1029/2010GL045922, 2010.

732



- 733 Miller, E. S., Makela, J. J., and Kelley, M. C., Seeding of equatorial plasma depletions by
734 polarization electric fields from middle latitudes: Experimental evidence, *Geophys. Res.*
735 *Lett.*, 36, L18105, doi:10.1029/2009GL039695, 2009.
- 736
- 737 Munro, G. H., Heisler, L. H.: Cusp-Type Anomalies in Variable Frequency Ionospheric
738 Records, *Austr. J. of Physics*, V.9 (3), 343-358, 1956.
- 739
- 740 Nishioka, M., Otsuka, Y., Shiokawa, K., Tsugawa, T., Effendy, Supnithi, P., Nagatsuma, T. and
741 Murata, K. T.: On post-midnight field-aligned irregularities observed with a 30.8-MHz radar at a
742 low latitude: Comparison with F-layer altitude near the geomagnetic equator, *J. Geophys. Res.*,
743 117, A08337, 732 doi:10.1029/2012JA017692, 2012.
- 744
- 745 Paulino, I., Medeiros, A. F., Buriti, R. A., Sobral, J. H. A., Takahashi, H., Gobbi, D.: Optical
746 observations of plasma bubble westward drift over Brazilian tropical region, *J. Atmos. Terr.*
747 *Phys.*, V. 72 (5-6), 521-27, 2010.
- 748
- 749 Paulino, I., Medeiros, A. F., Vadas, S., Wrasse, C. M., Takahashi, H., Buriti, R. A., Leite,
750 D., Figueira, S., Bageston, J. V., Sobral, J.H.A., and Gobbi, D.: Periodic waves in the lower
751 thermosphere observed by OI630nm airglow images. *Ann. Geophys.*, 34, 293–301, 2016.
- 752
- 753 Pimenta, A. A.; Amorim, D., Candido, C. M. N.: Thermospheric dark band structures at low
754 latitudes in the Southern Hemisphere under different solar activity conditions: A study using
755 OI 630 nm emission all-sky images, *Geophys. Res. Lett.*, 35, p. L16103,
756 doi:10.1029/2008GL034904, 2008.
- 757



758 Ratcliffe, J. A.: Some Irregularities in the F2 Region of the Ionosphere, *J. Geophys. Res.*,
759 50(4), 487-507, 1956.

760

761 Reinisch, B.W., Abdu, M. A., Batista, I. S., Sales, G. S., Khmyrov, G., Bullett, T. A., Chau,
762 T. and Rios V.: Multistation digisonde observations of equatorial spread F in South
763 America, *Ann. Geophys.*, 22, 3145–3153, 2004.

764

765 Reinisch, B.W., X. Huang, I.A. Galkin, V. Paznukhov, A. Kozlov: Recent advances in the
766 real-time analysis of ionograms and ionospheric drift measurements with digisondes, *J.*
767 *Atmos. Terr. Phys.*, 67 (2005) 1054–1062, (2005).

768

769 Sahai, Y.; Fagundes, P. R.; Bittencourt, J. A: Transequatorial F-region ionospheric plasma
770 bubbles solar cycle effects, *Journal of Atmospheric and Solar-Terrestrial Physics*, 62: 1377-
771 1383, 2000.

772

773 Shiokawa, K., Ihara, C., Otsuka, Y., Ogawa, T.: Statistical study of nighttime medium-scale
774 traveling ionospheric disturbances using midlatitude airglow images, *J. Geophys. Res.*, 108
775 (A1), 2003.

776

777 Sobral, J. H. A., Abdu, M. A.; Takahashi, H.; Taylor, M. J.; de Paula, E. R.; Zamlutti, C. J.;
778 Aquino, M. G.; Borba, G. L.: Ionospheric plasma bubble climatology over Brazil based on
779 22 years (1977-1998) of 630 nm airglow observations, *Journal of Atmospheric and Solar-*
780 *Terrestrial Physics*, 64: 1517-1524, 2002.

781



782 Sobral, J. H. A. et al.: Midnight reversal of ionospheric plasma bubble eastward velocity to
783 westward velocity during geomagnetically quiet time: Climatology and its model validation,
784 J. Atmos. Terr. Phys., 73, 1520–1528, 2002.

785

786 Valladares, C. E., Hanson, W. B., McClure, J. P., Cragin, B.L.: Bottomside sinusoidal
787 irregularities in the equatorial F region, Journal of Atm. and Solar-Terr Phys, V. 88 (A10),
788 <https://doi.org/10.1029/JA088iA10p08025>, 1983.

789

790 Yokoyama, T., Yamamoto, M., Otsuka, Y., Nishioka, M., Tsugawa, T., Watanabe, S. and
791 Pfaff, R. F.: On post-midnight low latitude ionospheric irregularities during solar minimum:
792 1. Equatorial Atmosphere Radar and GPS TEC observations in Indonesia, J. Geophys. Res.,
793 116, A11325, doi:10.1029/2011JA016797, 2011.

794

795

796

797

798

799

800

801

802

803

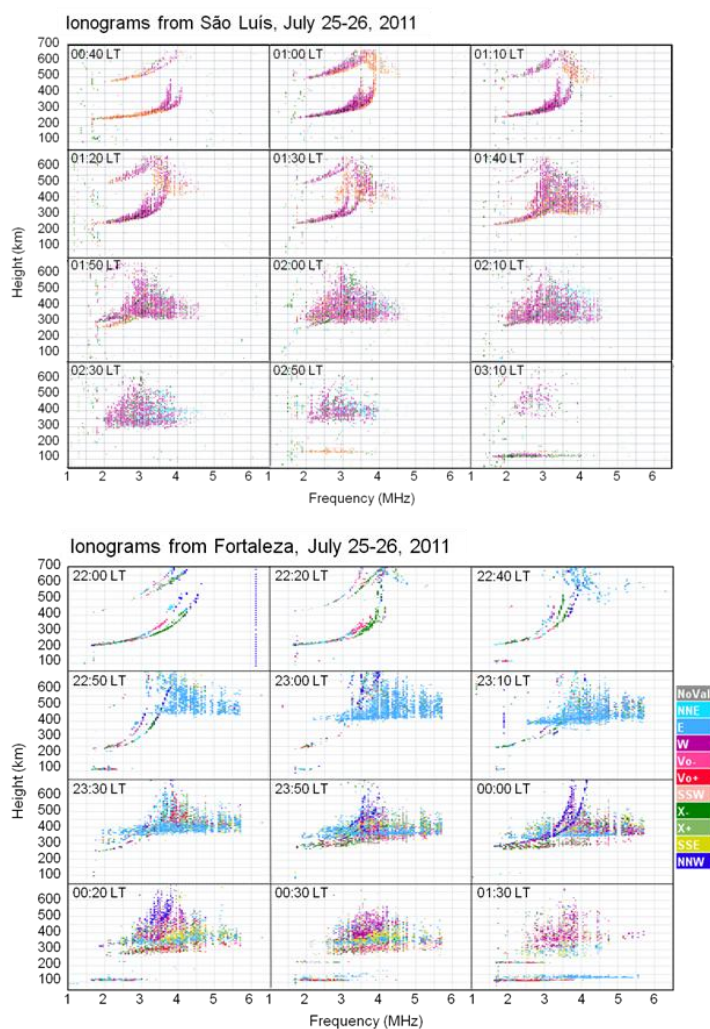
804

805

806



807 Figure 1



808

809

810 **Figure 1:** Sequence of ionograms obtained on July 25-26, at São Luís, from 00:40 to 03:10

811 LT and over FZ, Brazil, 2011, from 22:00 to 01:30 LT. The spread-F shows an unusual

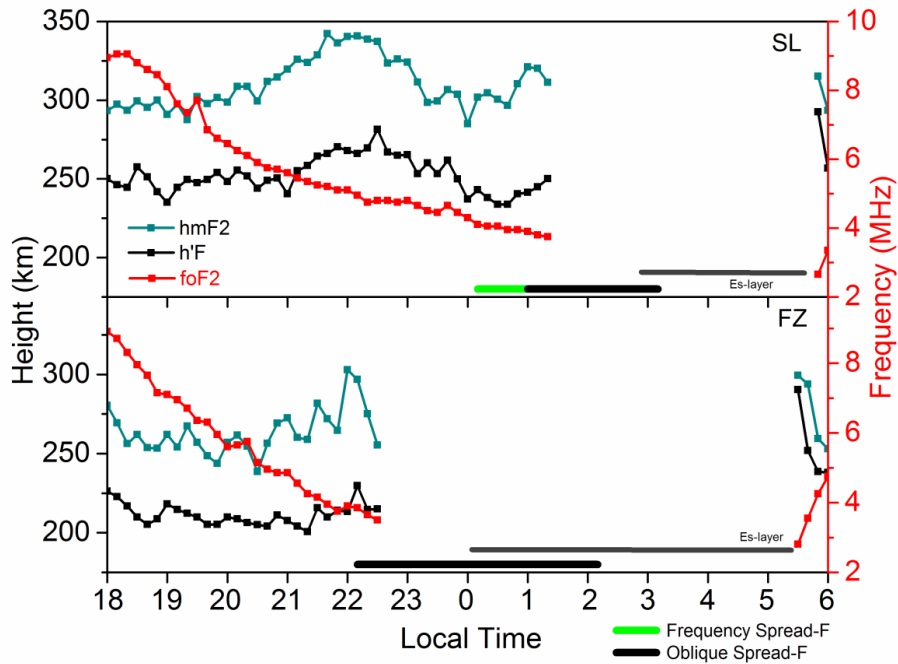
812 pattern, with oblique echoes. The color scale in FZ ionograms indicates echoes are coming

813 from the east and propagating to the westward.

814



815 Figure 2



816

817 **Figure 2:** F-layer parameters $h'F$ (km), hmF2 (km) and foF2 (MHz), on July 25-26, 2011

818 obtained from the Digisondes at São Luis and Fortaleza.

819

820

821

822

823

824

825

826

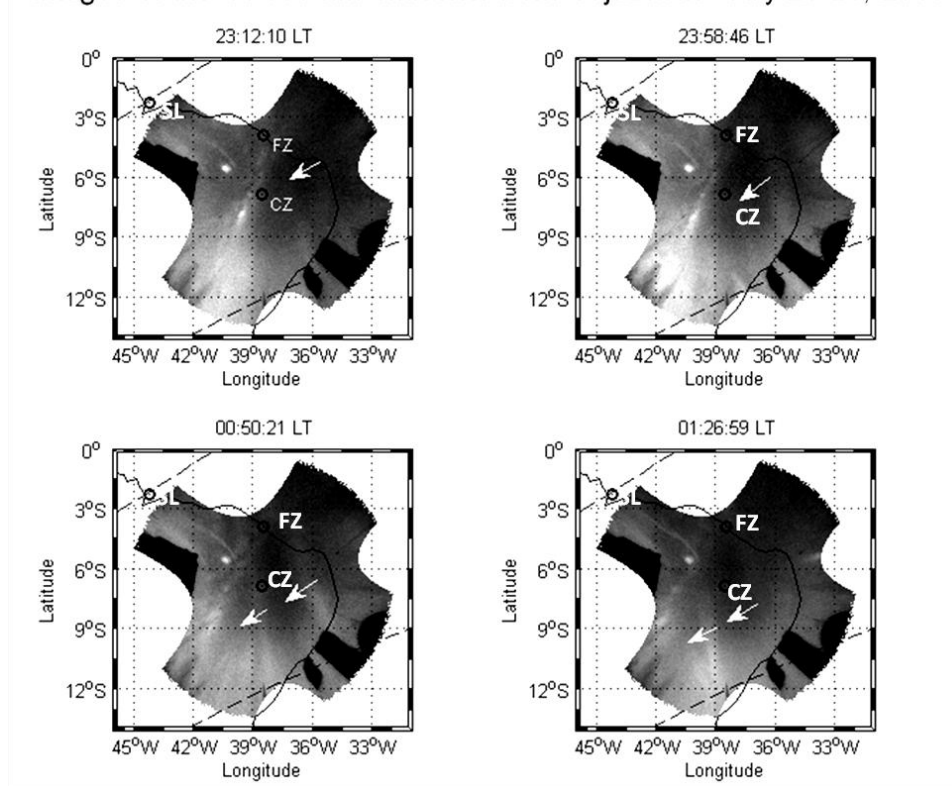
827



828 Figure 3

829

Images of the OI 630-nm emission from Cajazeiras July 25-26, 2011



830

831 **Figure 3:** Sequence of OI 630-nm images showing the time evolution of depletions on July
832 25-26, 2011, between 23:12 LT and 01:26 LT at Cajazeiras, Brazil. The images are
833 projected onto geographic coordinates over the Brazil map. In the plot, FZ is Fortaleza, SL
834 is Sao Luis, and CZ is Cajazeiras. Arrows indicate the propagation direction of the
835 depletions.

836

837

838

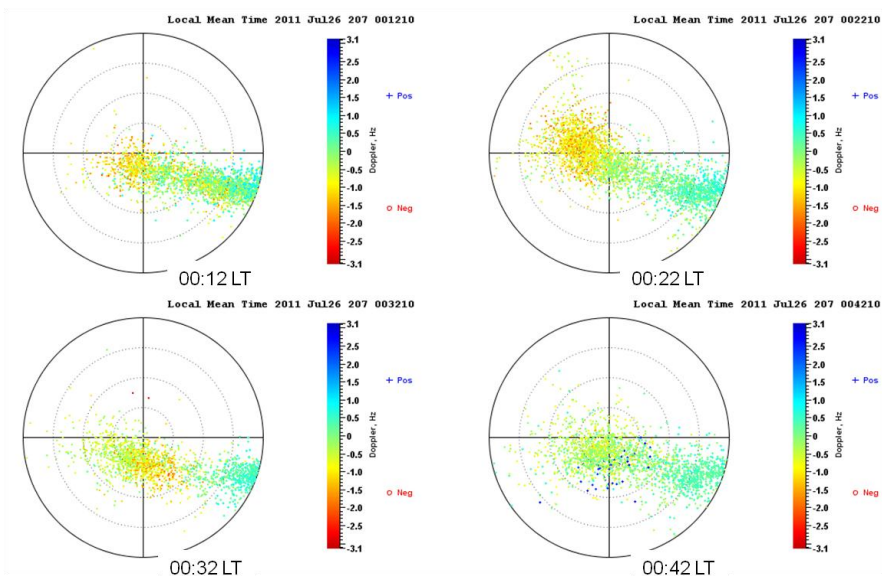
839



840 Figure 4

841

Skymaps from Fortaleza on July 25-26, 2011



842

843

844 **Figure 4:** Skymaps registered over FZ from 00:12 LT to 00:42 LT on July 26, 2011,

845 showing the echoes location and Doppler frequencies (color-coded) for F-region

846 echoes from Digisondes. Doppler velocities: Positive: irregularities arriving at the

847 station; Negative: irregularities leaving the station.

848

849

850

851

852

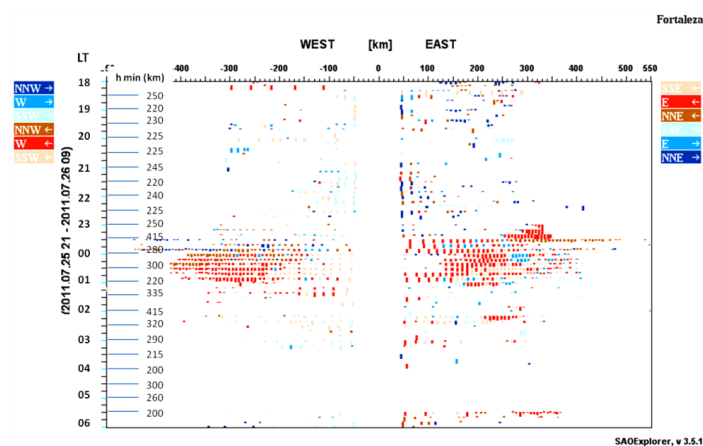
853

854



855

856 Figure 5



857

858 **Figure 5:** Directogram for Fortaleza on July 26 showing the location and the horizontal
859 distances of the irregularities detected by Digisonde and seen in the ionograms as spread-F.
860 At left: F-region height (km), where hmin is spread-F reflection height.

861

862

863

864

865

866

867

868

869

870

871

872

873

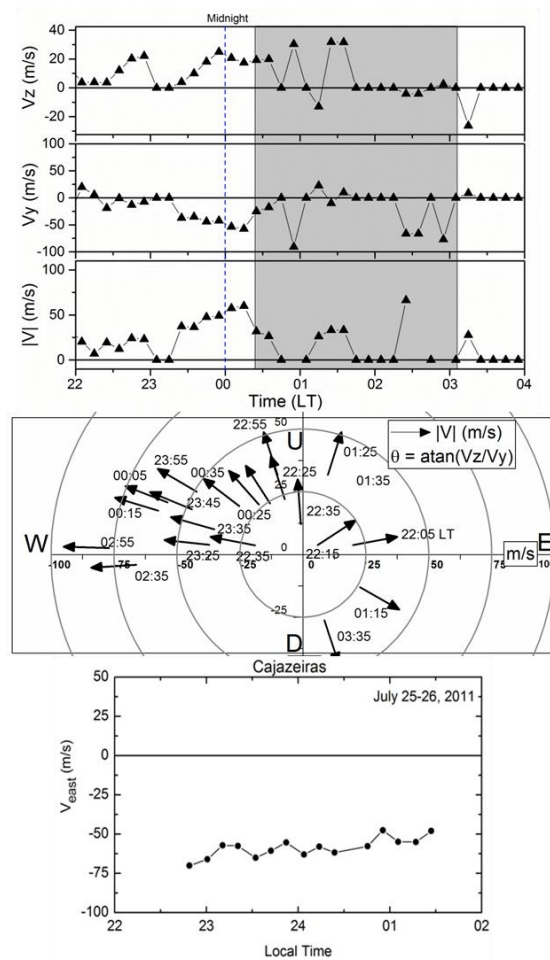


874

875

876 Figure 6

877

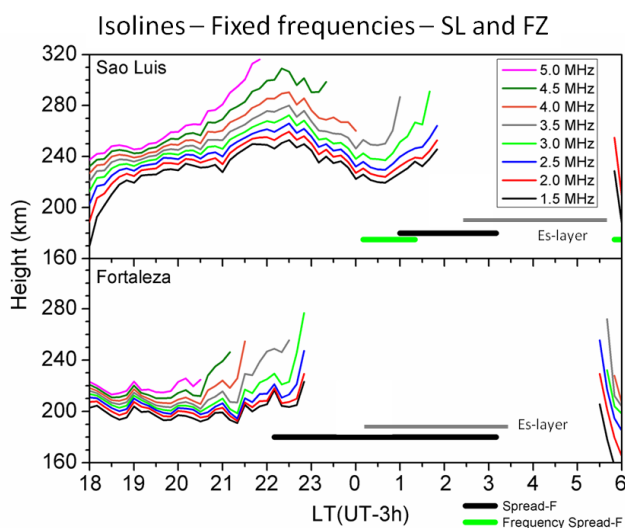


878

879 **Figure 6:** Top Panel: Vertical (V_z) and zonal drift (V_y) velocities on July 25-26, 2011 over
 880 FZ from 22:00 LT to 04:00 LT. $V_{\text{east}} > 0$. Middle Panel: Vector diagram showing the
 881 variations and directions of the mean total drift velocity of the irregularities seen as spread-F
 882 in ionograms. For clarity, the $|V|$ values are represented by the arrow start points. Bottom



883 panel: Zonal drift velocities obtained from the depletions seen on the OI 630.0 nm emission
884 images obtained at CZ on July 25-26, 2011 for comparison.
885
886

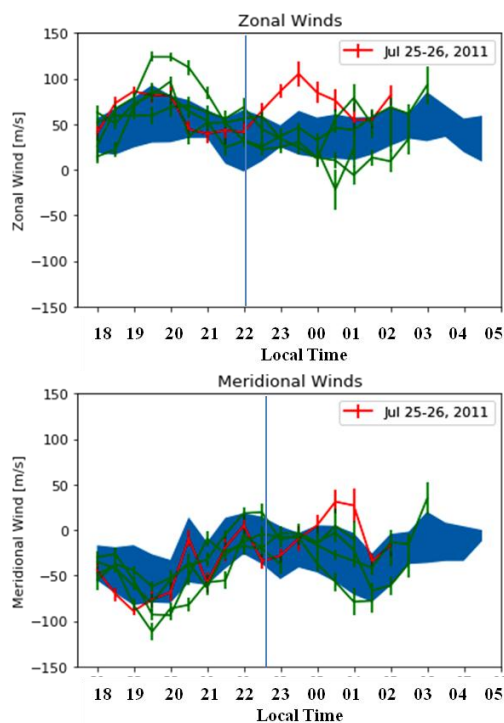


887
888 **Figure 7:** Oscillations in the real height of F-layer, at fixed frequencies during the spread-F
889 in São Luis (top panel) and Fortaleza (bottom panel).

890
891
892
893
894
895
896
897
898
899



900



901

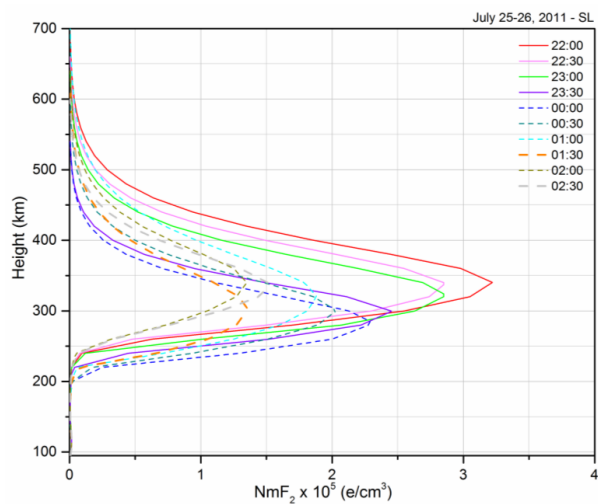
902 Figure 8: Measured Zonal and Meridional Winds in CZ, Brazil, in July 2011. The shaded
903 region is the monthly average, the green lines are the mean winds on July 25-26 (mean of 2
904 days), and the red line is for July 25-26.

905

906

907

908



909

910 Figure 9: F-layer plasma density profile for July 25-26, taken from Digisonde measurements

911 installed in SL, and by Sao-Explore inversion techniques.

912

913

914

915

916

917

918

919

920

921

922

923

924

925



926 **List of figures**

927

928 Figure 1: Sequence of ionograms obtained on July 25-26, at São Luis, from 00:40 to 03:10
929 LT and over FZ, Brazil, 2011, from 22:00 to 01:30 LT. The spread-F shows an unusual
930 pattern, with oblique echoes. The color scale in FZ ionograms indicates echoes are coming
931 from the east and propagating to the westward.

932

933 Figure 2: F-layer parameters $h'F$ (km), $hmF2$ (km) and $foF2$ (MHz), on July 25-26, 2011
934 obtained from the Digisondes at São Luis and Fortaleza.

935

936 Figure 3: Sequence of OI 630-nm images showing the time evolution of depletions on July
937 25-26, 2011, between 23:12 LT and 01:26 LT at Cajazeiras, Brazil. The images are
938 projected onto geographic coordinates over the Brazil map. In the plot, FZ is Fortaleza, SL
939 is Sao Luis, and CZ is Cajazeiras.

940

941 Figure 4: Skymaps registered over FZ from 00:12 LT to 00:42 LT on July 26, 2011,
942 showing the echoes location and Doppler frequencies (color-coded) for F-region echoes
943 from Digisondes. Doppler velocities: Positive: irregularities arriving at the station; Negative:
944 irregularities leaving the station.

945

946 Figure 5: Directogram for Fortaleza on July 26 showing the location and the horizontal
947 distances of the irregularities detected by Digisonde and seen in the ionograms as spread-F.
948 At left: F-region height.

949



950 Figure 6: Top Panel: Vertical (V_z) and zonal drift (V_y) velocities on July 25-26, 2011 over
951 FZ from 22:00 LT to 04:00 LT. $V_{\text{east}} > 0$. Middle Panel: Vector diagram showing the
952 variations and directions of the mean total drift velocity of the irregularities seen as spread-F
953 in ionograms. Bottom Panel: Zonal drift velocities obtained from the depletions seen on the
954 OI 630.0 nm emission images obtained at CZ on July 25-26, 2011.

955

956 Figure 7: Oscillations in the real height of F-layer, at fixed frequencies during the spread-F
957 in São Luis (top panel) and Fortaleza (bottom panel).

958

959 Figure 8: Measured Zonal and Meridional Winds in CZ, Brazil, in July 2011. The shaded
960 region is the monthly average, the green lines are the mean winds on July 25-26 (mean of 2
961 days), and the red line is for July 25-26.

962

963 Figure 9: F-layer plasma density profile for July 25-26.

964

965

966

967

968

969

970

971

972